PHYSICAL REVIEW C **105**, 064609 (2022)

Coherent description of elastic scattering and fusion at near-barrier energies for the ^{9}Be + ^{208}Pb and ^{9}Be + ^{197}Au reactions

K. Palli,[1,2] J. Casal,[3] and A. Pakou[1,*]

[1]*Department of Physics and HINP, The University of Ioannina, 45110 Ioannina, Greece*

[2]*Department of Chemistry, National and Kapodistrian University of Athens and HINP, 15771 Athens, Greece*

[3]*Departamento de Física Atómica, Molecular y Nuclear, Facultad de Física, Universidad de Sevilla, Apartado 1065, E-41080 Sevilla, Spain*

(Received 1 April 2022; accepted 1 June 2022; published 21 June 2022)

Elastic scattering, total reaction, and fusion cross sections of the systems ^{9}Be + ^{208}Pb and ^{9}Be + ^{197}Au at near-barrier energies, are coherently analyzed into two theoretical contexts. In a phenomenological approach, a BDM3Y1 interaction is used in an optical model potential analysis of the elastic-scattering data and the energy dependence of the potential is mapped around the Coulomb barrier. In a second approach, the elastic scattering is investigated within a four body framework by using the continuum-discretized coupled-channels method. In both scenarios, total reaction cross sections are determined and compared with phenomenological predictions. Moreover, an effective potential is obtained and in a one barrier penetration model analysis, the fusion excitation function is determined and compared with experimental data, further validating our analysis.

DOI: 10.1103/PhysRevC.105.064609

I. INTRODUCTION

Elastic scattering and fusion are the most appropriate observables for probing effectively coupling channel effects, which appear strong around barrier. Subsequently, the description of such observables can be made either via coupled-channel theories, or with phenomenological effective potentials, extracted through the energy dependence of the various optical model parameters. Both these approaches will be used in this work, studying the systems ^{9}Be + ^{208}Pb and ^{9}Be + ^{197}Au and will be validated via existing experimental data and vice versa.

For stable systems the energy variation of the potential parameters in a phenomenological approach appears at barrier, as a localized peak in the strength of the real potential. This is associated with a sharp decrease in the strength of the imaginary potential, as the various reaction channels are closing down. The effect is known as potential threshold anomaly [1,2]. The significance of this phenomenon, revealed by elastic-scattering data, is demonstrated in the interpretation of data in other reaction channels. In fact in the subbarrier and near-barrier energy region, fusion data for stable nuclei have been reproduced [1,3] by using a barrier penetration model with an energy dependent potential corresponding to the threshold anomaly.

For weakly bound projectiles the phenomenon of the threshold anomaly is not fully clarified. For the lithium projectiles, ^{6}Li and ^{7}Li the situation is diverting. For ^{6}Li, we observe a new anomaly(see, e.g., Refs. [4–22]) with an increasing imaginary potential approaching barrier from higher to lower energies and dropping to zero at deep subbarrier energies. For ^{7}Li on the other hand, the energy evolution of the imaginary potential resembles that of well bound nuclei. In the energy dependence of the real part however, a smoother peak develops or remains flat, especially for light targets. For ^{9}Be the data for the energy dependence of the potential are scarce [23–25]. In Ref. [23] the energy dependence of the potential at below and near-barrier energies is sought for light targets as ^{27}Al and ^{28}Si and a similar behavior is found, as for ^{7}Li but with a slower drop of the imaginary potential to zero. The same is found for a ^{208}Pb target in Ref. [24] but contradictory for the same target in Ref. [25] and for a ^{209}Bi target in Ref. [26]. For a ^{197}Au target, in Ref. [27], the drop of the imaginary potential to zero occurs at very low subbarrier energies. In this respect, in the present study, the energy dependence of the potential for ^{9}Be will be sought in a coherent analysis for two heavy targets, namely, ^{208}Pb and ^{197}Au, at near and below barrier energies in a global Optical Model Potential approach (OMP). Elastic-scattering data, reported in Refs. [24,25,27], will be considered and will be fit in a BDM3Y1 framework for probing the energy dependence of the potential and for determining total reaction cross sections. The latter will be compared with phenomenological predictions reported in Ref. [28]. Further on, the obtained energy dependence of the potential will be used in a standard one Barrier Penetration Model (BPM) approach [1–3,29,30], for determining fusion cross sections. These will be compared with data reported in Refs. [31–34]. Our BPM model describes fusion, as the absorption induced by a local model optical potential with the real part incorporating the energy dependence as determined from elastic-scattering fits. The imaginary part has a short range so that absorption does not occur until the barrier has been traversed. This is equivalent to imposing an in-going wave boundary condition inside the barrier (IWBC) [35].

---

[*] Corresponding author: apakou@uoi.gr

The ^{9}Be nucleus is a Borromean nucleus, attracting strong interest due to its three-body structure (α-α-n) or/and the two-body modes (^{5}He + ^{4}He, ^{8}Be + n) leading also to three body, with serious implications on astrophysical problems [36]. A predominance of the ^{5}He + ^{4}He mode, inferred by structural studies in Ref. [37] and verified experimentally in Refs. [38–41], was adopted with some success in coupled-channel calculations in Ref. [42] for ^{9}Be + ^{208}Pb. Coupling channel effects were also considered in fusion data with ^{9}Be on various targets but taking into account the two-body structure ^{8}Be + n, failing to reproduce the data in Ref. [43]. With the advent of four body continuum discretized coupled-channel (CDCC) calculations the problem has been addressed by using the analytical transformed harmonic oscillator for the three-body method [36,44]. CDCC calculations in a four body approach [36,45,46] have been applied on elastic scattering for ^{9}Be on ^{27}Al, ^{28}Si, ^{120}Sn, and ^{208}Pb targets [23,47–49]. In the present study, similar four body CDCC calculations will be applied coherently for the systems ^{9}Be + ^{197}Au and ^{9}Be + ^{208}Pb in a global approach. In this respect, total reaction cross sections will be extracted and compared with phenomenological predictions [28]. Further on, under the same CDCC formalism the dynamic polarization potential (DPP) will be derived, following the prescription of Thompson *et al.* [50], as applied in Ref. [51]. Subsequently, with the effective potential (bare + DPP) BPM fusion cross sections will be calculated in the standard way, as an additional observable for evaluating our calculations versus the elastic-scattering data and vice versa. Similarly to the phenomenological description, the imaginary part of the potential would be a Woods Saxon one, confined inside the barrier radius, simulating the in-going wave boundary conditions [52].

The structure of this paper goes as follows: Section II describes the phenomenological analysis and includes the OMP analysis, the energy dependence of the optical potential together with the dispersion predictions, as well as the fusion and total reaction cross-section comparisons. Section III includes our CDCC theory in a four-body formalism, with results on elastic scattering, total reaction cross sections, and breakup cross sections. Fusion cross sections will be extracted in a BPM formalism. All observables will be compared with the data. In Sec. IV, we present a discussion of our results together with our concluding remarks.

II. THE PHENOMENOLOGICAL ANALYSIS

The phenomenological analysis is a coherent analysis of existing elastic-scattering and fusion data for ^{9}Be + ^{197}Au and ^{9}Be + ^{208}Pb as well as of existing phenomenological total reaction cross-section predictions. It includes an optical model potential analysis of elastic scattering for probing the energy dependence of the potential and therefore the coupling channel mechanisms. Fusion and total reaction cross sections act as restrictions to the OMP analysis. Within this spirit we present below the specific parts of this study.

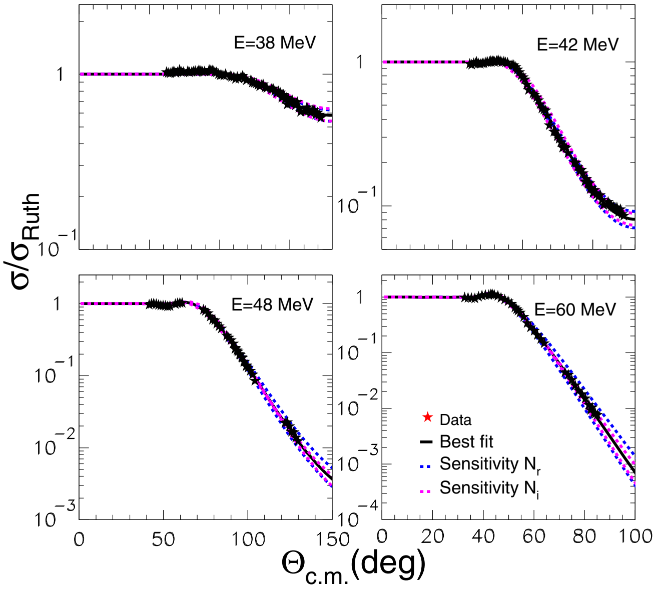

FIG. 1. Sample elastic-scattering data for ^{9}Be + ^{208}Pb, reported by Woolliscroft *et al.* [24]. The solid lines are the best fits in our BDM3Y1 analysis. Other lines refer to our sensitivity analysis, for extracting the uncertainty in the potential parameters N_R and N_i (see text).

A. Optical model potential analysis

The OMP calculations were consistently performed with the code ECIS [53] for all data sets. The real part of the entrance potential was calculated within the double folding model [54] by using the BDM3Y1 interaction developed by Khoa *et al.* [55]. Hartree-Fock calculations obtained by Trache *et al.* [56] were adopted for the ^{9}Be density, involved in the real double-folded potential. For the targets, the densities were obtained from electron-scattering data, adopting a standard procedure with a three parameter Fermi model, suitably corrected to derive a matter density from the empirical charge density. The same folded potential was adopted for the imaginary part of the potential with a different normalization factor. This proved to be a more flexible procedure, tested before with ^{6}Li elastic-scattering data [6].

In Fig. 1, we present sample elastic-scattering data for ^{9}Be + ^{208}Pb obtained by Woolliscroft *et al.* [24] at four energies together with the fits and a sensitivity analysis performed for extracting the error of the potential parameters. The sensitivity analysis includes a grid search, where at certain values of the real normalization factor of the BDM3Y1 interaction, below and above the best fit value, the normalization factor of the imaginary potential is searched, such as to fit the data. The same is repeated with the normalization factor for the imaginary part of the potential. In Fig. 2, we present the energy evolution of these parameters as a function of the energy versus the Coulomb barrier. The latter was extracted as $V_{\text{C.b.}}^{\text{lab}} = 41.2$ MeV, adopting the Broglia relation [57]. The deduced total reaction cross sections are included in Table I, together with the phenomenological predictions, reported in Ref. [28], and are found in excellent agreement with them.

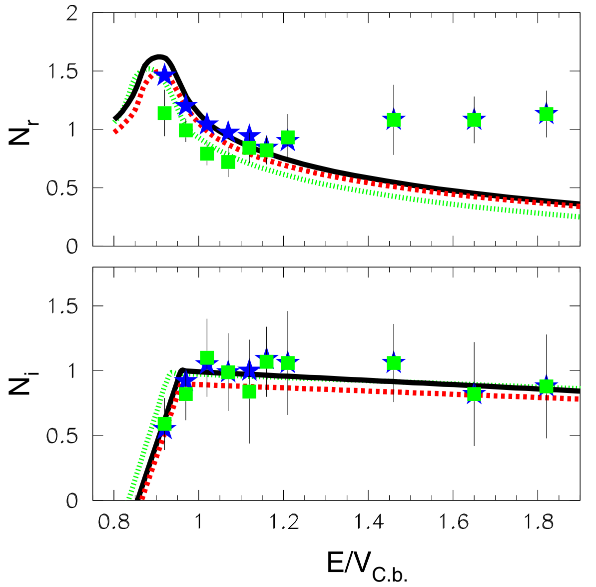

FIG. 2. The energy dependence of the optical potential for $^{9}\mathrm{Be}+{}^{208}\mathrm{Pb}$. The Coulomb barrier in the laboratory is taken as $V_{\mathrm{C.b.}}^{\mathrm{lab}}=41.2$ MeV, according to Broglia [57]. Data designated with the green cubes are extracted via a best fit to elastic scattering data. Data designated with the blue stars are due to a restricted calculation for compatibility with the fusion cross sections (see blue dashed curve in Fig. 6). The black line represents dispersion calculations according to Ref. [60] by using for the imaginary potential a two-segment method [7]. The sensitivity of the choice of linear segments, is also demonstrated with various other lines.

Subsequently we follow the same procedure with the elastic-scattering data, reported by Yu *et al.* in Ref. [25] for the same system. Sample elastic-scattering data with the best fits are shown in Fig. 3. The obtained total reaction cross sections have been included in Table II. We observe that at the lower energies these values are far from the phenomenological predictions of Ref. [28]. The energy evolution of the obtained normalization factors are displayed in Fig. 4, in comparison with those extracted from the data of Woolliscroft *et al.* [24]. The energy evolution at the lower energies is markedly diverting from the data of Woolliscroft *et al.* [24]. The imaginary part starts to decrease, then shows an increasing trend. In relation with it, the real part while starts to increase, then starts to decrease. This energy dependence deduced from the Yu *et al.* data does not follow any standard trend of weakly bound nuclei neither of ^{7}Be or ^{7}Li not even of ^{6}Li (see, e.g., Ref. [23]). In the case of ^{6}Li we have an increasing behavior as we approach barrier but this is connected with an almost flat behavior of the real part and a peak appearing at deep subbarrier energies (see, e.g., Refs. [4,19,23]). The real part of the potential as extracted by the Yu data below barrier (4 to 5 energy points) appear more repulsive than attractive as supposed to be in order to comply with a fusion enhancement. The difference between the elastic-scattering angular distributions of the two elastic-scattering data sets at lower energies of Woolliscroft *et al.* and Yu *et al.* is displayed, for 38 MeV, in Fig. 5. This difference inevitably leads to different normalization factors and therefore optical potentials. Taking into account two criteria for the validity of the one or the other set of data, that is the noncompatibility of deduced total reaction cross sections with predictions extracted from systematics and the nonphysical energy evolution of the potential, we conclude that the data of Woolliscroft *et al.* present a more coherent behavior than the Yu data, and in the following we concentrate on the data of Woolliscroft *et al.* for $^{9}\mathrm{Be}+{}^{208}\mathrm{Pb}$.

TABLE I. Total reaction cross sections extracted from the best fits for $^{9}\mathrm{Be}+{}^{208}\mathrm{Pb}$ elastic-scattering data, reported previously in Ref. [24] are designated as σ_{fit}, and are compared with phenomenological predictions, σ_{pre}, reported before in Ref. [28] with parameters $\hbar\omega=4.704$, $V_b=39.17$ MeV, and $R_b=11.35$ fm. In the fourth column appear total reaction cross sections σ_{restr} extracted by fitting only the imaginary part of the potential while keeping fixed the real normalization factor such as to represent well the fusion cross sections—see the blue dot-dashed line in Fig. 6. In the final column we present results σ_{final}, taking into account the dispersive potential described in Fig. 2 with the solid black line.

E_{lab} (MeV)	σ_{fit} (mb)	σ_{pre} (mb)	σ_{restr} (mb)	σ_{final} (mb)
38	98.9	105	98	123
40	265	303	235	323
42	482	512	480	504
44	636	706	714	685
46	811	883	850	853
48	1035	1046	1018	1008
50	1165	1194	1193	1150
60	1823	1791	1809	1709
68	2144	2141	2083	2025
75	2384	2387	2337	2239

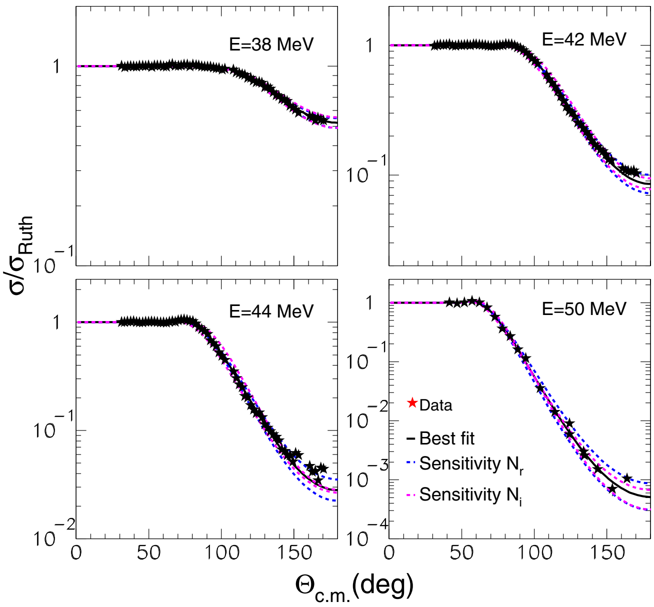

FIG. 3. Sample elastic-scattering data for $^{9}\mathrm{Be}+{}^{208}\mathrm{Pb}$ reported by Yu *et al.* [25]. The solid lines are the best fits in our BDM3Y1 analysis. Other lines refer to our sensitivity analysis for extracting the uncertainty in the potential parameters N_R and N_i (see text).

TABLE II. Total reaction cross sections extracted from the best fits for ^{9}Be + ^{208}Pb elastic-scattering data, reported previously in Ref. [25] by Yu *et al.*, are designated as $\sigma_{\rm fit}$, and are compared with phenomenological predictions, $\sigma_{\rm pre}$, reported before in Ref. [28] with parameters $\hbar\omega = 4.704$, $V_b = 39.17$ MeV, and $R_b = 11.35$ fm.

$E_{\rm lab}$ (MeV)	$\sigma_{\rm fit}$ (mb)	$\sigma_{\rm pre}$ (mb)
37.8	148	89
38	155	105
38.2	163	121
38.5	184	148
38.7	189	167
39	214	197
39.5	259	249
40	310	303
41	406	409
42	503	512
44	691	707
47.2	969	982
50	1235	1194

An excitation function of fusion data, both complete fusion and total fusion, were reported before by Dasgupta *et al.* [31] and are presented in Fig. 6. The data are compared with Wong calculations as well as with BPM calculations with the code ECIS. In the BPM model the fusion cross section depends on the potential barrier, defined as the sum of the effective ^{9}Be + ^{208}Pb nuclear and Coulomb potentials. The calculation included the real part of the nuclear potential as deduced

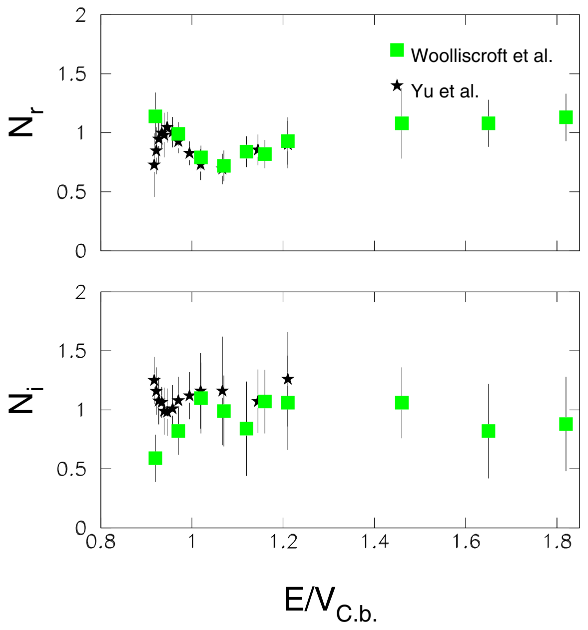

FIG. 4. The energy dependence of the optical potential for ^{9}Be + ^{208}Pb, extracted by the elastic-scattering data of Yu *et al.* [25]. The Yu *et al.* data are designated with the black stars and are compared with the Woolliscroft *et al.* data, designated by the green boxes. The Coulomb barrier in the laboratory is according to Broglia [57]; $V_{\rm C.b.}^{\rm lab} = 41.2$ MeV.

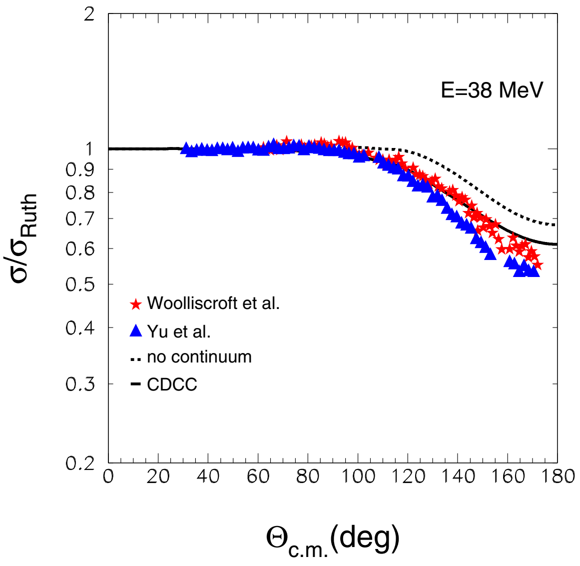

FIG. 5. Elastic-scattering data for ^{9}Be + ^{208}Pb at 38 MeV reported by Woolliscroft *et al.* [24], designated by the red stars, compared with data reported by Yu *et al.* [25], designated by the blue triangles. The lines correspond to our CDCC calculations (see Sec. III).

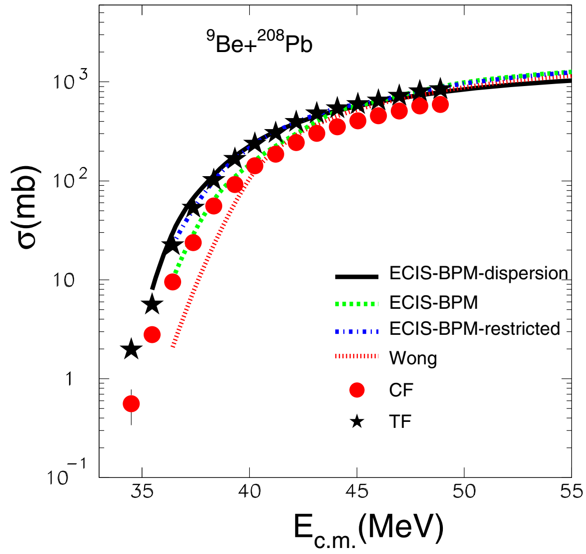

FIG. 6. Fusion cross sections for ^{9}Be + ^{208}Pb reported by Dasgupta *et al.* [31] are compared with our calculations. Complete fusion data (CF) are designated with red circles while total fusion data (TF) are designated with the black stars. Our calculations are (a) according to Wong, designated with the red dotted line, (b) according to one-barrier penetration model with the code ECIS, designated with the dashed green line and the label ECIS-BPM. (c) The ECIS-BPM-restricted calculation, designated with the dot-dashed blue line, is deduced by fixing the normalization factors of the real part of the potential such as to represent well the fusion data and (d) the BPM-ECIS-dispersion calculations were deduced with normalization factors, obtained by our dispersive calculations, and are designated with the solid black line—see black solid line in Fig. 2.

from fits to elastic-scattering data, while the imaginary, described with a Woods Saxon form factor, was arranged such as to absorb all the flux penetrating the barrier, simulating the in-going wave boundary conditions [30,58,59]. The relevant line in Fig. 6 is designated with the label ECIS-BPM dashed green line. As it is seen this line describes adequately well the data but underpredict them below barrier. In this respect, we have searched for new normalization factors of the real part of the potential such as to probe in the best way the fusion data, designated in Fig. 6, by the dot-dashed blue line labeled as restricted. The corresponding normalization factors are included in Fig. 2. The new normalization factors are consistent with the “original” of the best fit ones, into a reasonable uncertainty, and we will adopt this potential parameters from now on. Note that the obtained total reaction cross sections, in this “restricted” fit are included in Table I, and show a good consistency with the best fit and predicted values. Therefore, we conclude here that within the error, the energy-dependent potential can well describe both fusion data as well as total reaction cross sections of phenomenological predictions (see also our results in the Sec. II B).

The same procedure as above was then followed for the system $^{9}\mathrm{Be}+{}^{197}\mathrm{Au}$. However, the fit to elastic-scattering data at the below-barrier energies was unattainable, giving unphysical normalization factors. Therefore we changed the philosophy of our analysis adopting the following steps and assuming that fusion measurements are accurate:

(1) Determine the normalization factors for the real part of the potential with the restriction that, BPM calculations with the code ECIS (see above) can reproduce the total fusion data [32]. See the blue dot-dashed line in Fig. 7.

(2) Fix the normalizations of the real part to the values obtained in step 1 and then fit the elastic-scattering data with only one free parameter, the normalization factors of the imaginary potential. Put a restriction to this fit such as the total reaction cross sections to be compatible with the phenomenological predictions of Ref. [28] (see Table III). The results of the energy dependence of the potential are displayed in Fig. 8, while sample elastic-scattering data are compared with the calculations in Fig. 9.

In Fig. 9, the solid black line represents the best fit, but giving unphysical normalization factors, while the dot-dashed blue line reflects the above calculations. Big deviations from the best fit are mainly seen at the lower energies and more profoundly for the energy at 36 MeV, perhaps due to inherent problems in the measurement. We note here a usual problem on low-energy measurements at particular angles, with the reaction products recoiling through very large distances inside the target, if the last is not tilted. Then, the dotted blue lines indicate possible corrections to the elastic-scattering data if we request a simultaneous consistency with total reaction cross sections and fusion cross sections. We should note here that, below barrier, the two existing sets of fusion measurements of Gollan *et al.* [32] and Kaushik *et al.* [33] are well compatible between themselves, validating this analysis. A third set of measurements of Li *et al.* [34], refer to above-barrier energies well compatible with the data of Kaushik *et al.* The Gollan *et al.* data above barrier present a suppression of 25% from BPM and Wong calculations not seen by the other sets. Therefore from now on we will consider as total fusion cross section data for $^{9}\mathrm{Be}+{}^{197}\mathrm{Au}$, the data sets of Kaushik *et al.* and Li *et al.* The main conclusion from the above analysis

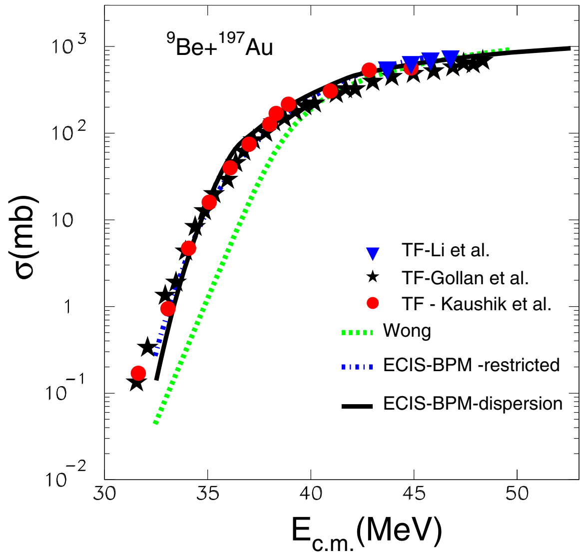

FIG. 7. Total fusion cross sections for $^{9}\mathrm{Be}+{}^{197}\mathrm{Au}$ reported by Gollan *et al.* [32], by Kaushik *et al.* [33], and by Li *et al.* [34] are compared with our calculations. Our calculations are (a) according to Wong, the green dotted line, (b) restricted to pass through the lower energy total fusion data—the dot-dashed blue line. The normalization factors of the real potential in the BPM calculation was fixed such as to reproduce the fusion data at least at the lower energies and (c) BPM calculations with ECIS (see text) designated with the solid black line, according to the dispersive potential—Fig. 8, black solid line.

TABLE III. Total reaction cross-section predictions for $^{9}\mathrm{Be}+{}^{197}\mathrm{Au}$, σ_{pre}, reported before in Ref. [28] with parameters $\hbar\omega = 4.673$ MeV, $V_b = 38.135$ MeV, and $R_b = 11.227$ fm are compared with present values, σ_{final}, deduced taking into account a dispersive potential described in Fig. 8 with the solid black line.

E_{lab} (MeV)	σ_{pre} (mb)	σ_{final} (mb)
34	4	
35	13	13
36	39	48
37	98	117
38	189	217
39	294	317
40	401	404
41	505	496
42	605	589
44	790	773
46	959	931
48	1113	1075

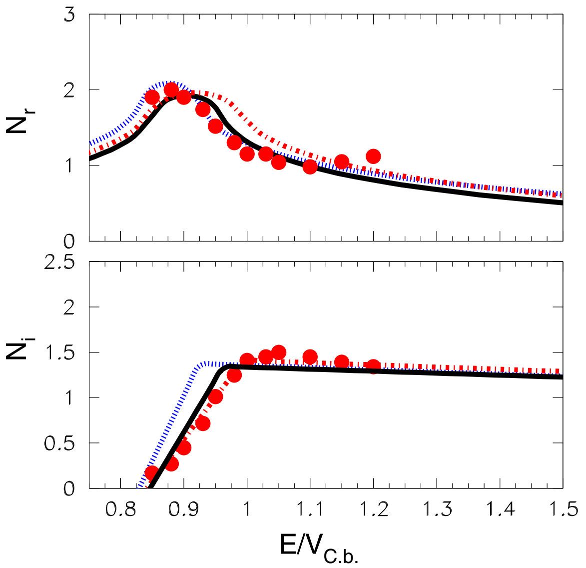

FIG. 8. The energy dependence of the optical potential for ^{9}Be + ^{197}Au. The Coulomb barrier in the laboratory was taken as $V_{\mathrm{C.b.}}^{\mathrm{lab}} = 40.2$ MeV, according to Broglia [57]. The lines represent dispersion relations according to Ref. [60], by using for the imaginary potential a two-segment method [7]. The solid black line represents the description of the potential compatible with both fusion data [32] and total reaction cross-section predictions [28]. Other lines are there to demonstrate the sensitivity of the choice of linear segments on the dispersive correction.

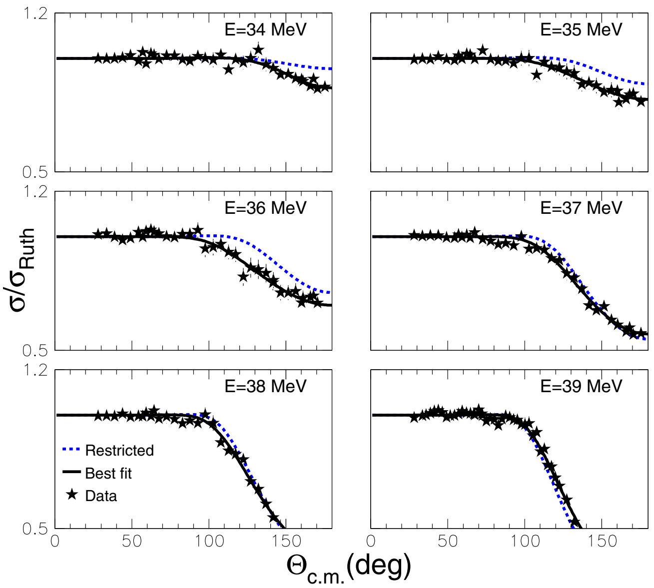

FIG. 9. Sample elastic-scattering data for ^{9}Be + ^{197}Au, reported by Gollan *et al.* [27]. The solid lines are the best fits in our BDM3Y1 analysis, but for the three lower energies giving unphysical normalization factors. The dot-dashed blue lines refer to elastic scattering with the appropriate potential such as to fulfill requirements relevant to fusion measurements [32] and total reaction cross-section predictions [28].

is that, meaningful results for the energy dependence of the optical potential at near and subbarrier energies can be drawn only if we can combine results of several experimental quantities. Of course elastic-scattering data of good precision are also useful in that direction.

B. The dispersive description

Reducing the many-body problem to a one-body problem, we adopt an effective interaction or optical potential, writing

$$U(r;E) = V(r;E) + iW(r;E), \tag{1}$$

where V and W are the real and imaginary parts related through the following dispersion relation in a subtracted form normalizing V$_0$ at some convenient energy E_s [60]

$$V(r;E) = V_0(r;E_s) + \frac{P}{\pi}(E-E_s)\int_0^\infty \frac{W(r;E')}{(E'-E_s)(E'-E)}dE'. \tag{2}$$

To apply the dispersion correction for the potential of ^{9}Be + ^{208}Pb, we have chosen two linear segments for representing the energy variation of the imaginary part of the potential (see in Fig. 2, solid black line). Two other sets of two segment lines were drawn to demonstrate the sensitivity of the dispersion correction on the choice of the imaginary part of the potential. The dispersive effect on the real part is determined through the analytical expression given in Ref. [1] and is displayed for the above system in Fig. 2. The same procedure was applied to the ^{9}Be + ^{197}Au data and the results are included in Fig. 8. Results for total reaction cross sections, adopting the dispersive potentials, are compared with systematics in Tables I and III for ^{9}Be + ^{208}Pb and ^{9}Be + ^{197}Au respectively and are found in very good agreement with the other values, as expected. Further on, adopting these potentials, BPM calculation are performed, for calculating total fusion for both systems (see Figs. 6 and 7). The corresponding results in a reduced form [61], are compared in Fig. 10 between themselves and the relevant data [31,32], as well as are compared with the Universal Fusion Function (UFF) curve. It is apparent, that the deviation of the data below barrier from the UFF curve, being due to coupling channel effects, is perfectly described by a BPM calculation, taking into account the energy dependence of the potential through dispersive relations.

III. THE CONTINUUM-DISCRETIZED COUPLED CHANNELS CALCULATIONS

Due to the weakly bound nature of the three-body ^{9}Be projectile, we studied the reaction dynamics within the four body CDCC framework. Calculations were performed as in Ref. [49], where ^{9}Be was described as an $\alpha + \alpha + n$ three-body system and the coupling to breakup channels was included explicitly. We should note here that by using an $\alpha + n + n$ three-body model for the projectile the possible configurations ^{8}Be $+n$ and ^{5}He + ^{4}He are implicitly included and treated consistently in our approach. The ^{9}Be internal Hamiltonian was solved using the hyperspherical description [36], generating the $3/2^-$ ground state and $j^\pi = 1/2^\pm$, $3/2^\pm$, $5/2^\pm$ continuum pseudostates. These states were employed to

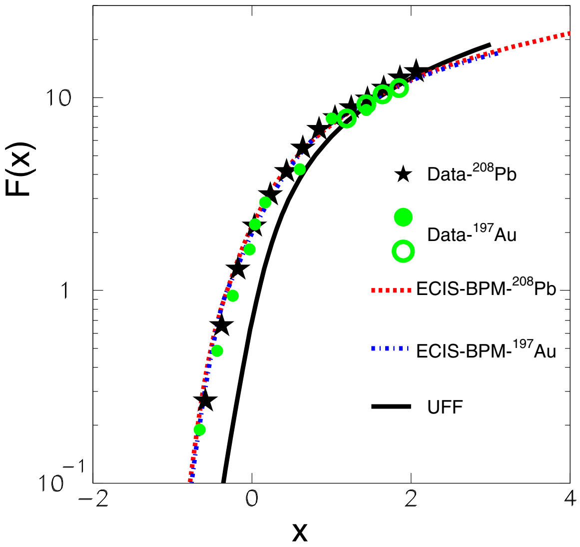

FIG. 10. Reduced total fusion data for ^{9}Be + ^{208}Pb [31] and ^{9}Be + ^{208}Au [33,34] are compared between themselves and our BPM calculations as well as with the UFF curve. For the BPM calculations the dispersive potentials, designated with the solid black lines in Figs. 2 and 8 are adopted.

compute the corresponding coupling potentials to all orders, using as ingredients n-target and α-target optical potentials. For the former, we fixed the Köning & Delaroche potential [62] at the proper energy/nucleon. For the latter, we tested several α-^{208}Pb potentials from the literature, finding the one in Ref. [63] to provide the best overall description of the elastic scattering, simultaneously, around the rainbow region and at backward angles. Note that this potential is different from the one used in Ref. [49]. For a coherent description, we used the same coupling potential for the ^{197}Au target. Then, the coupled-channels problem was solved up to convergence, inserting the generated coupling potentials in FRESCO [5]. In practice, relative projectile-target angular momenta up to $L = 150$ were included, and ^{9}Be excitations up to 8 MeV were required. It is worth noting that, once the structure input and optical potentials are fixed, the four body CDCC calculations are free from parameter fitting.

For a more global understanding of the effect of continuum on reaction channels, in addition to elastic-scattering distributions, total reaction, breakup cross sections and fusion cross sections in a BPM scenario were extracted, to be described in the following sections. The BPM calculations were performed adopting an ansatz for a barrier penetration model [23,52]. In this approach the fusion cross section depends on the Coulomb barrier, defined as the sum of the effective ^{9}Be + ^{208}Pb nuclear and Coulomb potentials. The effective nuclear potential was taken to be the sum of the bare potential and the dynamic polarization potential (DPP). The bare potential includes only the ground-state diagonal term. The dynamic polarization potential was derived from CDCC calculations following the prescription of Thompson *et al.* [50]. In the same way as in the phenomenological description, the imaginary part of the potential was such as to simulate the in-going wave boundary conditions [23].

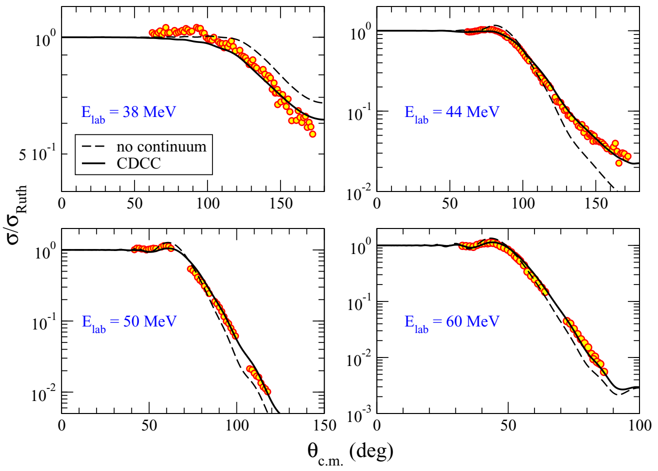

FIG. 11. CDCC calculations are compared with elastic-scattering data for ^{9}Be + ^{208}Pb and reported by Woolliscroft *et al.* [24].

A. The ^{9}Be + ^{208}Pb system

The elastic-scattering results are compared with angular distribution data for four energies, below and above barrier, in Fig. 11. The relevant breakup cross sections are compared with experimental data [64] in Fig. 12 and are included in Table IV. In the same table, the total reaction cross sections extracted into this formalism are compared with relevant values obtained in our OMP analysis and with phenomenological predictions. The agreement is very good, except for the value at the lower energy. Further on, the coupling to continuum seems to be moderately strong and capable for

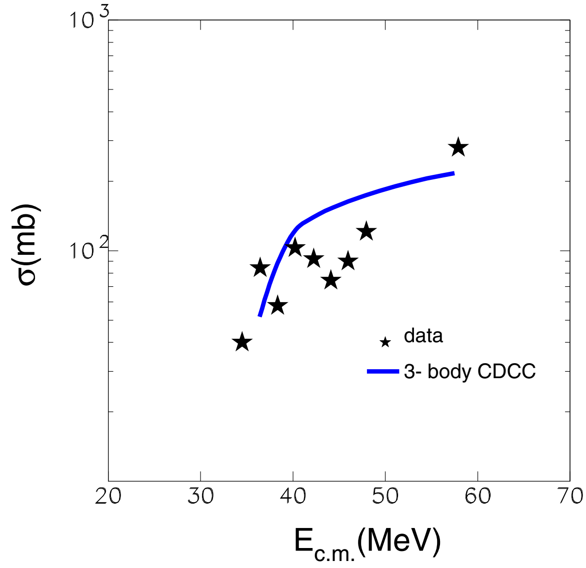

FIG. 12. CDCC calculations for the breakup of ^{9}Be + ^{208}Pb as a function of energy are compared with data, reported by Woolliscroft *et al.* [64].

TABLE IV. Total reaction cross section for ^{9}Be + ^{208}Pb obtained in our CDCC formalism are compared with our OMP analysis values, σ_{OMP} (see Table I, final values), and phenomenological predictions, σ_{pre} [28]. In the final column we present the breakup cross sections obtained in our CDCC formalism, σ_{break}.

E_{lab} (MeV)	σ_{cdcc} (mb)	σ_{OMP} (mb)	σ_{pre} (mb)	σ_{break} (mb)
38	218.4	123	105	51.7
42	586.8	504	512	123.1
44	771.1	685	706	139.4
48	1103.8	1008	1046	163.5
50	1249.8	1150	1194	173.7
60	1822.3	1709	1791	216.9

reproducing in an excellent way the elastic-scattering data. The agreement for breakup between calculation and experiment is also adequately good, taking into account the assumptions under which these data were determined. The energy dependence of the DPP is demonstrated in Fig. 13, for three distinct radii at $R = 12$, 12.4, and 13 fm, close to the radius $R = 12.3$ fm determined as the sensitivity radius in the OMP analysis, reported in Ref. [24]. According to our calculations this value corresponds to the strong absorption radius. Both real and imaginary part display a tendency, although weak, to become more negative at energies near and below barrier. This means that the real part of the bare potential will be increased at barrier and therefore this DPP is in accordance with a standard potential threshold anomaly, as already has been outlined in our OMP analysis and the analysis in Ref. [24]. The fact that this tendency is weak may indicate that other reaction processes are due, contributing to coupling channel effects. We should note here that this tendency continues until the radius of 11.4 fm, where we have a turning point and the DPP becomes more positive below barrier. However, we believe that this part of the potential does not contribute to the elastic scattering which is more located at the surface. It is interesting to note here that the more positive trend found in our analysis below 11.4 fm was found to be valid at the strong absorption radius, if a two-body structure for ^{9}Be is assumed (^{5}He + ^{4}He) in Ref. [42]. The BPM fusion results are compared with experimental data [31] in Fig. 14, exhibiting an adequate agreement with them. The slight underestimation of the data below barrier may indicate the presence of other reaction channels in addition to the direct excitation to continuum, which are needed to be taken consistently in a coupled-channel scheme. This is in accordance with our conclusion for the trend of the polarization potential in relation with the threshold anomaly (TA).

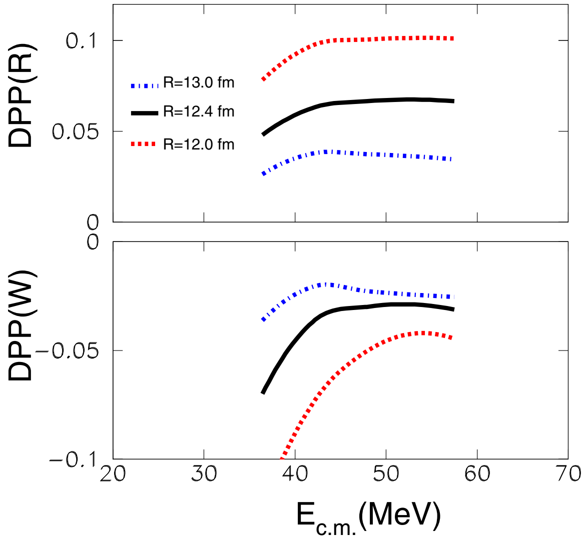

FIG. 13. DPP potentials for ^{9}Be + ^{208}Pb at three distinct radii $R = 12$, 12.4, and 13 MeV. These radii are close to the value 12.3 fm, determined in the OMP analysis of Ref. [24] as the sensitive radius. According to our analysis this corresponds to the strong absorption radius.

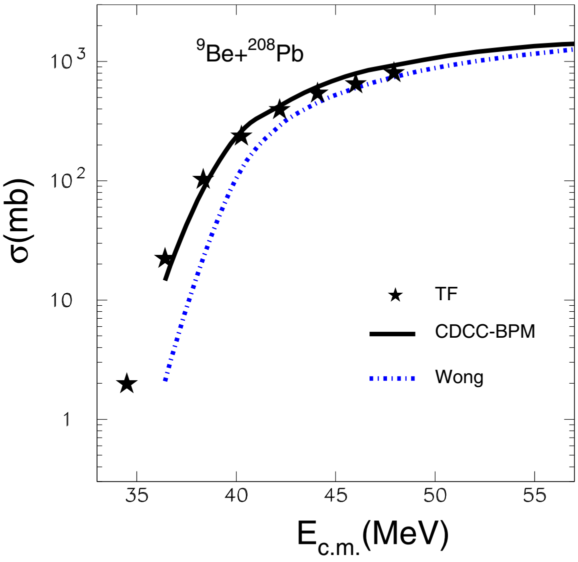

FIG. 14. Total fusion cross sections reported previously for ^{9}Be + ^{208}Pb by Dasgupta *et al.* [31] compared with our CDCC-BPM calculations (see text).

B. The ^{9}Be + ^{197}Au system

In general, the results of elastic scattering for ^{9}Be + ^{197}Au are included in Fig. 15, exhibiting a very good agreement with the data. A good compatibility is also seen among the total reaction cross sections deduced in this formalism, Table V, and the values extracted from our OMP analysis as well as values from the phenomenological prediction [28]. On the other hand, at the lower energy below barrier, we have, as in the case of the lead target, an obvious disagreement. This may have to do with a strong energy dependence of the coupling potentials below barrier not accommodated in the present calculations. For this system we have no breakup experimental data to compare with our CDCC calculations. It is interesting though to compare our results, see Fig. 16, with transfer data and incomplete fusion data (ICF), reported by Kaushik *et al.* in Ref. [33]. We see that both transfer and breakup have the

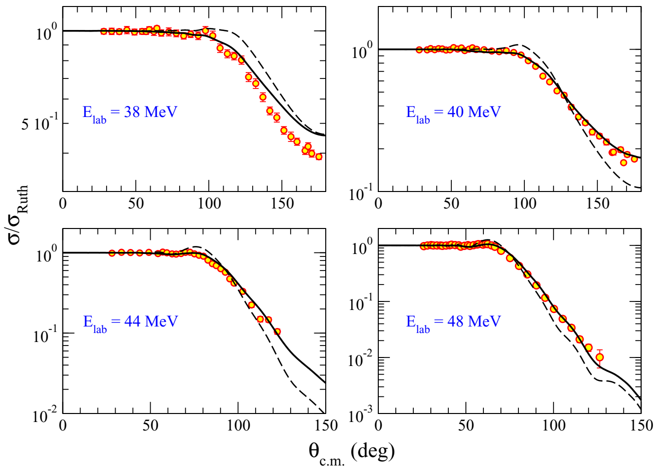

FIG. 15. CDCC calculations are compared with elastic-scattering data for ^{9}Be + ^{197}Au, reported by Gollan *et al.* [27].

same strength and play a major role at below-barrier energies. The question, if couplings to both these processes are equally important or not, cannot be replied by this simplified comparison. The fact that, above barrier, both processes have the same cross section as the ICF data cannot speak either for a one- or two-step fusion mechanism, but definitely speaks for the suppression of complete fusion due to either of these direct processes. More elaborate measurements or/and calculations are needed for delineating such issues (see, e.g., Refs. [65–68]).

The energy dependence of the DPP potentials extracted in our CDCC formalism for ^{9}Be + ^{197}Au is displayed in Fig. 17. Similar conclusions as in the ^{9}Be + ^{197}Au case can be drawn here as well. For the real part of DPP we observe a negative trend as we go to values below barrier. This is compatible with the peak appearing in TA. For the imaginary potential we note a small variation from the relevant plot for ^{208}Pb. Here the drop to zero is slower in accordance with our OMP analysis (compare Figs. 2 and 8).

Finally we present in Fig. 18, our BPM fusion results in comparison with total fusion cross sections reported in Refs. [33,34]. Below barrier the agreement is very good although we have no calculations at very low energies. Above barrier, we observe a small overestimation. Going back to the previous question in relation with the importance of couplings either to transfer or to breakup, we can say that coupling to breakup is in principle adequate to describe both elastic scattering and fusion. On the other hand our calculation cannot discriminate between direct breakup or breakup following transfer.

TABLE V. Total reaction cross section for ^{9}Be + ^{197}Au obtained in our CDCC formalism, are compared with our OMP analysis values, σ_{OMP} (see Table III, final values), and phenomenological predictions, σ_{pre} [28]. In the final column we present the breakup cross sections obtained in our CDCC formalism, σ_{break}.

E_{lab} (MeV)	σ_{cdcc} (mb)	σ_{OMP} (mb)	σ_{pre} (mb)	σ_{break} (mb)
38	267.6	189	217	87.2
40	425.8	401	404	107.2
44	853.1	790	773	139.0
48	1170.9	1113	1075	160.9

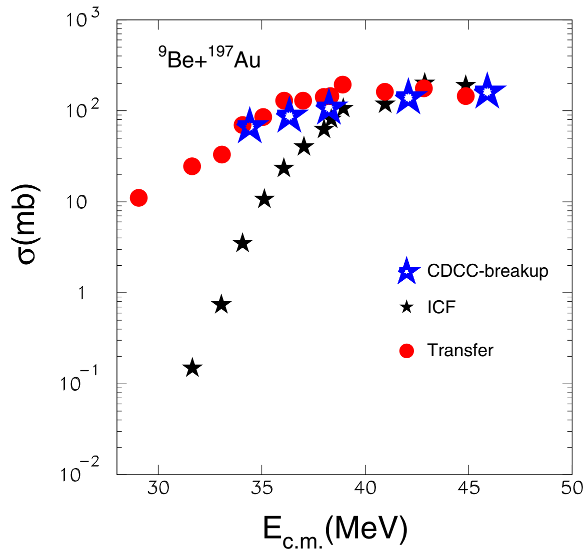

FIG. 16. CDCC calculations for the breakup of ^{9}Be + ^{197}Au as a function of energy are compared with data for incomplete fusion (ICF) and transfer reported by Kaushik *et al.* [33].

IV. SUMMARY AND CONCLUSIONS

Coupling channel effects were probed for the systems ^{9}Be + ^{208}Pb and ^{9}Be + ^{197}Au, in two scenarios. In the first scenario and the system ^{9}Be + ^{208}Pb, a coherent phenomenological analysis was performed taking into account previous

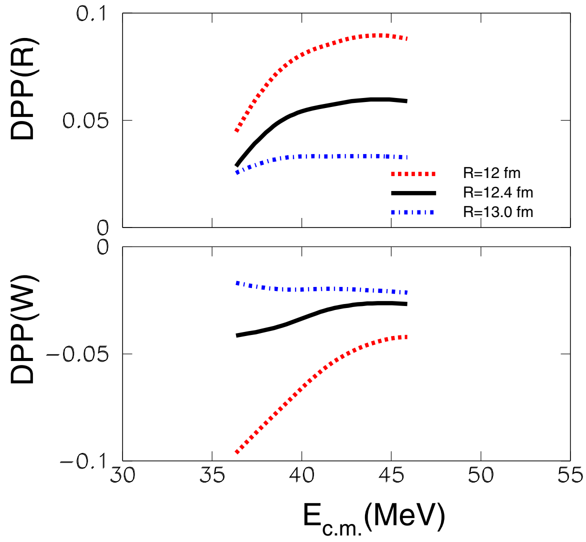

FIG. 17. DPP potentials for ^{9}Be + ^{197}Au, at three distinct radii $R = 12$, 12, 4 and 13 fm. These values are close to the strong absorption radius, determined in this work as $R_S = 12.2$ fm.

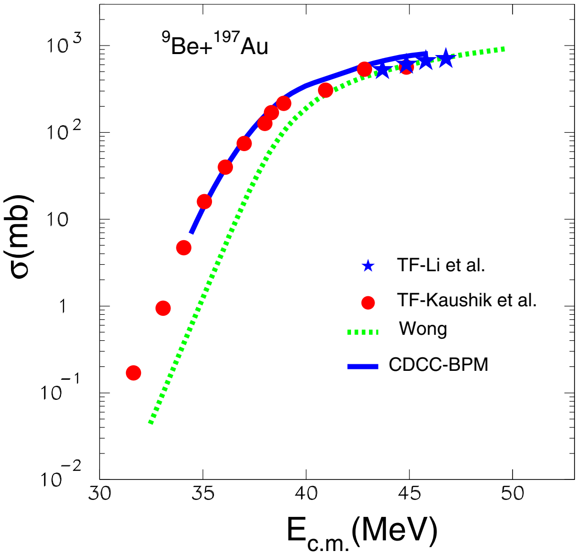

FIG. 18. Total fusion cross sections reported previously for ^{9}Be + ^{197}Au by Kaushik *et al.* [33] and Li *et al.* [34] are compared with our CDCC-BPM and Wong calculations (see text).

elastic-scattering and fusion data [24,31]. Total reaction cross-section predictions [28] were also used for validating our results. In our approach the energy dependence of the OMP potential was probed through fits to elastic-scattering data using a BDM3Y1 interaction. The real and imaginary part of the potential was successfully described via dispersion relations exhibiting the usual potential threshold anomaly (TA). The extracted total reaction cross sections were in excellent agreement with the predictions [28]. This energy-dependent potential was then used in a BPM model for describing fusion. Small deviations from the total fusion data were smoothed out by sequential fits until all data on elastic scattering, fusion, and total reaction cross sections were given a unique energy-dependent potential. This procedure was not possible follow for the data on ^{197}Au, due possibly to inherent problems with the measurement of elastic-scattering angular distributions at the energies below barrier. In this case, starting from the fusion measurements [32–34] and a BPM calculation we were able to determine the energy dependence of the real part of the OMP potential and subsequently the energy dependence of the imaginary coefficients through fits with the elastic-scattering data [27]. This fit was restricted by the total reaction predictions. In this approach the energy dependence of the OMP potential was also described by dispersive relations and a usual TA was probed. It is important to underline here, that taking into account the energy dependence of the potentials via the dispersive descriptions, our BPM calculations for fusion were found in excellent agreement with the relevant data and between themselves, if compared in a reduced form (see Fig. 10).

In the second scenario couplings to continuum were considered in a four-body CDCC approach. The same fragment-target optical potentials were used for both systems. Our elastic-scattering results indicate an excellent agreement with the experimental data. So did the deduced total reaction cross sections, compatible with both the OMP results and phenomenological predictions [28] but at the above-energy region. At below-barrier energies the deviations are large and have been attributed to a possible strong energy dependence of the coupling potentials not accommodated in the present description. Into the same formalism an effective potential was formed and fusion cross sections in a BPM approach was calculated, compared adequately well with the data. The extracted DPPs found to be compatible with the standard TA exhibited by both systems. This trend of the DPPs, however, was weak, indicating the existence of other mechanisms contributing in the coupling channel effects. In summary our conclusions are as follows:

(1) The energy dependence of the ^{9}Be + ^{208}Pb and ^{9}Be + ^{197}Au OMP potentials found to exhibit the standard TA anomaly of well-bound systems as well as of the ^{7}Li weakly bound nucleus. However, the drop of the imaginary part of the potential may occur earlier or later of the barrier depending on the target and thus the reactions involved. In our case the drop for the lead target occurred earlier than in the case of the gold one. The above conclusions, based on the evaluation of several observables, clarify previous inconsistencies.

(2) For obtaining a trustworthy energy dependence of OMP at near-barrier energies, it is necessary the consideration of several observables and not solely fits to elastic scattering data. At these energies the Coulomb potential is substantial and overwhelming the nuclear one. Then fits to elastic-scattering data are not sensitive enough to the nuclear potential parameters.

(3) In general fusion data for weakly bound nuclei as ^{9}Be, can be described adequately well within a BPM approach, if the energy dependence of the OMP potential is taken into account. It is apparent here as in the case of well bound nuclei and suggested by Satchler and collaborators, that the enhancement of fusion can be regarded as another aspect of the optical potential threshold anomaly both being the manifestation of the same phenomenon, the coupling channel effects.

(4) A four-body approach in a CDCC framework, using THO wave functions, is necessary and in principle adequate for reactions at near-barrier energies, involving three-body projectiles as ^{9}Be.

(5) Couplings to continuum proved to be moderately strong but capable to describe elastic-scattering data at near-barrier energies. So did for sub- and near-barrier total fusion data via the extracted DPPs in a BPM approach. Small deviations between calculations and the fusion data may indicate the necessity of involving other reaction mechanisms in a more comprehensive coupled-channel formalism.

(6) Indications have been given, through the energy evolution of the dynamic polarization potential, that the observed potential threshold anomaly for ^{9}Be is mainly due to couplings on continuum excitations.

ACKNOWLEDGMENTS

We warmly thank Nicolas Alamanos, Krzysztof Rusek, Antonio Moro, and Manuela Rodríguez-Gallardo for valuable discussions. J.C. is supported by MCIN/AEI/10.13039/501100011033 under I + D + i Project No. PID2020-114687GB-I00, and by Consejería de Economía, Conocimiento, Empresas y Universidad, Junta de Andalucía and "ERDF-A Way of Making Europe" under PAIDI 2020 Project No. P20_01247.

---

[1] G. R. Satchler, Phys. Rep. **199**, 147 (1991).
[2] M. A. Nagarajan, C. C. Mahaux, and G. R. Satchler, Phys. Rev. Lett. **54**, 1136 (1985).
[3] M. A. Nagarajan and G. R. Satchler, Phys. Lett. B **173**, 29 (1986).
[4] N. Keeley, S. J. Bennett, N. M. Clarke, B. R. Fulton, G. Tungate, P. V. Drumm, M. A. Nagarajan, and J. S. Lilley, Nucl. Phys. A **571**, 326 (1994).
[5] A. M. M. Maciel, P. R. S. Gomes, J. Lubian, R. M. Anjos, R. Cabezas, G. M. Santos, C. Muri, S. B. Moraes, R. L. Neto, N. Added, N. C. Filho, and C. Tenreiro, Phys. Rev. C **59**, 2103 (1999).
[6] A. Pakou, N. Alamanos, A. Lagoyannis, A. Gillibert, E. C. Pollacco, P. A. Assimakopoulos, G. Doukelis, K. G. Ioannides, D. Karadimos, D. Karamanis, M. Kokkoris, E. Kossionides, N. G. Nicolis, C. Papachristodoulou, N. Patronis, G. Perdikakis, and D. Pierroutsakou, Phys. Lett. B **556**, 21 (2003).
[7] A. Pakou, N. Alamanos, G. Doukelis, A. Gillibert, G. Kalyva, M. Kokkoris, S. Kossionides, A. Lagoyannis, A. Musumarra, C. Papachristodoulou, N. Patronis, G. Perdikakis, D. Pierroutsakou, E. C. Pollacco, and K. Rusek, Phys. Rev. C **69**, 054602 (2004).
[8] J. M. Figueira, D. Abriola, J. O. Fernández Niello, A. Arazi, O. A. Capurro, E. de Barbará, G. V. Martí, D. Martínez Heimann, A. J. Pacheco, J. E. Testoni, I. Padrón, P. R. S. Gomes, and J. Lubian, Phys. Rev. C **73**, 054603 (2006).
[9] M. S. Hussein, P. R. S. Gomes, J. Lubian, and L. C. Chamon, Phys. Rev. C **73**, 044610 (2006); **76**, 019902(E) (2007).
[10] J. M. Figueira, O. Fernandez Niello, D. Abriola, A. Arazi, O. A. Capurro, E. de Barbara, G. V. Marti, D. Martinez Heimann, A. E. Negri, A. J. Pacheco, I. Padron, P. R. S. Gomes, J. Lubian, T. Correa, and B. Paes, Phys. Rev. C **75**, 017602 (2007).
[11] F. A. Souza, L. A. S. Leal, N. Carlin, M. G. Munhoz, R. Liguori Neto, M. M. de Moura, A. A. P. Suaide, E. M. Szanto, A. Szanto de Toledo, and J. Takahashi, Phys. Rev. C **75**, 044601 (2007); **76**, 029901(E) (2007).
[12] M. Biswas, S. Roy, M. Sinha, M. K. Pradhan, A. Mukherejee, P. Basu, H. Majumdar, K. Ramachandran, and A. Shrivastava, Nucl. Phys. A **802**, 67 (2008).
[13] H. Kumawat, V. Jha, B. J. Roy, V. V. Parkar, S. Santra, V. Kumar, D. Dutta, P. Shukla, L. M. Pant, A. K. Mohanty, R. K. Choudhury, and S. Kailas, Phys. Rev. C **78**, 044617 (2008).
[14] M. Zadro, P. Figuera, A. Di Pietro, F. Amorini, M. Fisichella, O. Goryunov, M. Lattuada, C. Maiolino, A. Musumarra, V. Ostashko, M. Papa, M. G. Pellegriti, F. Rizzo, D. Santonocito, V. Scuderi, and D. Torresi, Phys. Rev. C **80**, 064610 (2009).
[15] K. Zerva, A. Pakou, K. Rusek, N. Patronis, N. Alamanos, X. Aslanoglou, D. Filipescu, T. Glodariu, N. Keeley, M. Kokkoris, M. La Commara, A. Lagoyannis, M. Mazzocco, N. G. Nicolis, D. Pierroutsakou, and M. Romoli, Phys. Rev. C **82**, 044607 (2010).
[16] J. M. Figueira, J. O. Fernandez Niello, A. Arazi, O. A. Capurro, P. Carnelli, L. Fimiani, G. V. Marti, D. Martinez Heimann, A. E. Negri, A. J. Pacheco, J. Lubian, D. S. Monteiro, and P. R. S. Gomes, Phys. Rev. C **81**, 024613 (2010).
[17] N. N. Deshmukh, S. Mukherjee, D. Patel, N. L. Singh, P. K. Rath, B. K. Nayak, D. C. Biswas, S. Santra, E. T. Mirgule, L. S. Danu, Y. K. Gupta, A. Saxena, R. K. Choudhury, R. Kumar, J. Lubian, C. C. Lopes, E. N. Cardozo, and P. R. S. Gomes, Phys. Rev. C **83**, 024607 (2011).
[18] S. Santra, S. Kailas, K. Ramachandran, V. V. Parkar, V. Jha, B. J. Roy, and P. Shukla, Phys. Rev. C **83**, 034616 (2011).
[19] K. Zerva, A. Pakou, N. Patronis, P. Figuera, A. Musumarra, A. Di Pietro, M. Fisichella, T. Glodariu, M. La Commara, M. Latuada, M. Mazzocco, M. G. Pellegtiti, D. Pierroutsakou, A. M. Sanchez-Binitez, V. Scuderi, E. Strano, and K. Rusek, Eur. Phys. J. A **48**, 102 (2012).
[20] L. Fimiani, J. M. Figueira, G. V. Martí, J. E. Testoni, A. J. Pacheco, W. H. Z. Cárdenas, A. Arazi, O. A. Capurro, M. A. Cardona, P. Carnelli, E. de Barbará, D. Hojman, D. Martinez Heimann, and A. E. Negri, Phys. Rev. C **86**, 044607 (2012).
[21] V. Morcelle *et al.*, Phys. Rev. C **89**, 044611 (2014).
[22] S. Dubey, S. Mukherjee, D. C. Biswas, B. K. Nayak, D. Patel, G. K. Prajapati, Y. K. Gupta, B. N. Joshi, L. S. Danu, S. Mukhopadhyay, B. V. John, V. V. Desai, S. V. Suryanarayana, R. P. Vind, N. N. Deshmukh, S. Appnnababu, and P. M. Prajapati, Phys. Rev. C **89**, 014610 (2014).
[23] A. Pakou, O. Sgouros, V. Soukeras, J. Casal, and K. Rusek, Eur. Phys. J. A **58**, 8 (2022).
[24] R. J. Woolliscroft, B. R. Fulton, R. L. Cowin, M. Dasgupta, D. J. Hinde, C. R. Morton, and A. C. Berriman, Phys. Rev. C **69**, 044612 (2004).
[25] N. Yu, H. Q. Zhang, H. M. Jia, S. T. Zhang, M. Ruan, F. Yang, Z. D. Wu, X. X. Xu, and C. L. Bai, J. Phys. G **37**, 075108 (2010).
[26] C. Signorini, A. Andrighetto, M. Ruan, J. Y. Guo, L. Stroe, F. Soramel, K. E. G. Lobner, L. Muller, D. Pierroutsakou, M. Romoli, K. Rudolph, I. J. Thompson, M. Trotta, A. Vitturi, R. Gernhauser, and A. Kastenmuller, Phys. Rev. C **61**, 061603(R) (2000).
[27] F. Gollan, D. Abriola, A. Arazi, M. A. Cardona, E. de Barbará, D. Hojman, R. M. Id Betan, G. V. Martí, A. J. Pacheco, D. Rodrigues, and M. Togneri, Nucl. Phys. A **1000**, 121789 (2020).
[28] A. Pakou *et al.*, Eur. Phys. J. A **51**, 55 (2015).
[29] L. C. Vaz, J. M. Alexander, and E. H. Auerbach, Phys. Rev. C **18**, 820 (1978).
[30] M. J. Rhoades-Brown and P. Braun-Munzinger, Phys. Lett. B **136**, 19 (1984).
[31] M. Dasgupta, P. R. S. Gomes, D. J. Hinde, S. B. Moraes, R. M. Anjos, A. C. Berriman, R. D. Butt, N. Carlin, J. Lubian, C. R. Morton, J. O. Newton, and A. Szanto de Toledo, Phys. Rev. C **70**, 024606 (2004).
[32] F. Gollan, D. Abriola, A. Arazi, M. A. Cardona, E. de Barbará, J. de Jesús, D. Hojman, R. M. Id Betan, J. Lubian, A. J. Pacheco,

B. Paes, D. Schneider, and H. O. Soler, Phys. Rev. C **104**, 024609 (2021).

[33] M. Kaushik, S. K. Pandit, V. V. Parkar, G. Gupta, S. Thakur, V. Nanal, H. Krishnamoorthy, A. Shrivastava, C. S. Palshetkar, K. Mahata, K. Ramachandran, S. Pal, R. G. Pillay, and P. P. Singh, Phys. Rev. C **104**, 024615 (2021).

[34] G. S. Li, J. G. Wang, J. Lubian, H. O. Soler, Y. D. Fang, M. L. Liu, N. T. Zhang, X. H. Zhou, Y. H. Zhang, B. S. Gao, Y. H. Qiang, S. Guo, S. C. Wang, K. L. Wang, K. K. Zheng, R. Li, and Y. Zheng, Phys. Rev. C **100**, 054601 (2019).

[35] C. H. Dasso, S. Landowne, and A. Winther, Nucl. Phys. A **405**, 381 (1983).

[36] J. Casal, M. Rodríguez-Gallardo, J. M. Arias, and I. J. Thompson, Phys. Rev. C **90**, 044304 (2014).

[37] K. Arai, Y. Ogawa, Y. Suzuki, and K. Varga, Phys. Rev. C **54**, 132 (1996).

[38] A. Pakou, O. Sgouros, V. Soukeras, and F. Cappuzzello, Eur. Phys. J. A **57**, 25 (2021).

[39] A. Pakou, O. Sgouros, V. Soukeras, F. Cappuzello, L. Acosta, C. Agodi, S. Calabrese, D. Carbone, M. Cavallaro, I. Martel, A. M. Sánchez-Benítez, G. Souliotis, A. Spatafora, and D. Torresi, Nucl. Phys. A **1008**, 122155 (2021).

[40] A. Pakou *et al.*, Phys. Rev. C **101**, 024602 (2020).

[41] V. Soukeras, O. Sgouros, A. Pakou, F. Cappuzzello, J. Casal, C. Agodi, G. A. Brischetto, S. Calabrese, D. Carbone, M. Cavallaro, I. Ciraldo, I. Dimitropoulos, S. Koulouris, L. La Fauci, I. Martel, M. Rodríguez-Gallardo, A. M. Sánchez-Benítez, G. Souliotis, A. Spatafora, and D. Torresi, Phys. Rev. C **102**, 064622 (2020).

[42] N. Keeley, N. Alamanos, K. Rusek, and K. W. Kemper, Phys. Rev. C **71**, 014611 (2005).

[43] V. Jha, V. V. Parkar, and S. Kailas, Phys. Rev. C **89**, 034605 (2014).

[44] J. Casal, M. Rodríguez-Gallardo, and J. M. Arias, Phys. Rev. C **88**, 014327 (2013).

[45] M. Rodríguez-Gallardo, J. M. Arias, J. Gómez-Camacho, R. C. Johnson, A. M. Moro, I. J. Thompson, and J. A. Tostevin, Phys. Rev. C **77**, 064609 (2008).

[46] M. Rodríguez-Gallardo, J. M. Arias, J. Gómez-Camacho, A. M. Moro, I. J. Thompson, and J. A. Tostevin, Phys. Rev. C **80**, 051601(R) (2009).

[47] P. Descouvemont, T. Druet, L. F. Canto, and M. S. Hussein, Phys. Rev. C **91**, 024606 (2015).

[48] A. Arazi, J. Casal, M. Rodríguez-Gallardo, J. M. Arias, and R. Lichtenthäler Filho, Phys. Rev. C **97**, 044609 (2018).

[49] J. Casal, M. Rodríguez-Gallardo, and J. M. Arias, Phys. Rev. C **92**, 054611 (2015).

[50] I. J. Thompson, Comput. Phys. Rep. **7**, 167 (1988).

[51] K. Rusek and K. W. Kemper, Phys. Rev. C **61**, 034608 (2000).

[52] K. Rusek, N. Alamanos, N. Keeley, V. Lapoux, and A. Pakou, Phys. Rev. C **70**, 014603 (2004).

[53] J. Raynal, Phys. Rev. C **23**, 2571 (1981).

[54] G. R. Satchler and W. G. Love, Phys. Rep. **55**, 183 (1979).

[55] D. T. Khoa and W. von Oertzen, Phys. Lett. B **342**, 6 (1995).

[56] L. Trache, A. Azhari, H. L. Clark, C. A. Gagliardi, Y. W. Lui, A. M. Mukhamedzhanov, R. E. Tribble, and F. Carstoiu, Phys. Rev. C **61**, 024612 (2000).

[57] R. A. Broglia and A. Winther, *Heavy Ion Reactions, Volume I: Elastic and Inelastic Reactions* (The Benjamin/Cummings Publishing Company, Inc., San Francisco, 1981).

[58] N. Alamanos, Eur. Phys. J. A **56**, 212 (2020).

[59] D. M. de Castro Rizzo and N. Alamanos, Nucl. Phys. A **443**, 525 (1985).

[60] C. Mahaux, H. Ngo, and G. R. Satchler, Nucl. Phys. A **449**, 354 (1986).

[61] L. F. Canto, P. R. S. Gomes, J. Lubian, L. C. Chamon, and E. Crema, J. Phys. G **36**, 015109 (2009).

[62] A. J. Koning and J. P. Delaroche, Nucl. Phys. A **713**, 231 (2003).

[63] G. Goldring, M. Sanuel, B. A. Watson, M. C. Bertin, and S. L. Tabor, Phys. Lett. B **32**, 465 (1970).

[64] R. J. Woolliscroft, N. M. Clarke, B. R. Fulton, R. L. Cowin, M. Dasgupta, D. J. Hinde, C. R. Morton, and A. C. Berriman, Phys. Rev. C **68**, 014611 (2003).

[65] R. Rafiei, R. du Rietz, D. H. Luong, D. J. Hinde, M. Dasgupta, M. Evers, and A. Diaz-Torres, Phys. Rev. C **81**, 024601 (2010).

[66] K.J. Cook, E.C. Simpson, L.T. Bezzina, M. Dasgupta, D.J. Hinde, K. Banerjee, A.C. Berriman, and C. Sengupta, Phys. Rev. Lett. **122**, 102501 (2019).

[67] J. Lei and A. M. Moro, Phys. Rev. Lett. **123**, 232501 (2019).

[68] A. Shrivastava, A. Navin, N. Keeley, K. Mahata, K. Ramachandran, V. Nanal, V. V. Parkar, A. Chatterjee, and S. Kailas, Phys. Lett. B **633**, 463 (2006).